

Self-Organized Superlattice Formation during Crystal Growth from Continuous Beam Fluxes

Y. L. Foo,* K. A. Bratland, B. Cho, C. W. Lim, J. Baker, J. G. Wen, D. W. Moon,† and J. E. Greene

*Frederick Seitz Materials Research Laboratory and the Materials Science Department, University of Illinois,
104 South Goodwin Avenue, Urbana, Illinois 61801, USA*

(Received 10 March 2003; published 11 June 2003)

Alloy superlattice structures consisting of alternating Si-rich and C-rich layers form spontaneously during gas-source molecular beam epitaxy of $\text{Si}_{1-y}\text{C}_y$ on Si(001) from constant Si_2H_6 and CH_3SiH_3 precursor fluxes at $T_s = 725\text{--}750^\circ\text{C}$. The self-organized patterning is due to a complex interaction among competing surface reactions. During growth of the initial Si-rich layer, strain-driven C segregation to the subsurface results in charge transfer from surface Si atom dangling bonds to C backbonds. This decreases the Si_2H_6 sticking probability, and, hence, the instantaneous deposition rate, thereby enhancing C segregation. The Si-rich layer continues until a critical C coverage is reached allowing nucleation of a C-rich layer which grows until the excess subsurface C is depleted. The process then repeats with periods tunable through the choice of T_s and y_{avg} .

DOI: 10.1103/PhysRevLett.90.235502

PACS numbers: 81.07.-b, 61.46.+w, 81.15.Hi, 81.16.Dn

Self-organized processes during crystal growth are currently of intense interest in thin film science and technology. Examples include kinetically driven self-assembled mound and ripple structures during low-temperature homoepitaxy [1–3], strain-driven quantum dot formation [4–9], and one-dimensional quantum wires whose separation is controlled by the substrate vicinality [10–12]. There is, however, another level of self-organization that has not been widely exploited, the growth of self-assembled superlattices.

Highly ordered superlattices used in electronic, optical, and mechanical devices are presently produced artificially from alternating beam sources during growth by molecular beam epitaxy (MBE) [13], chemical vapor deposition [14], and sputter deposition [15]. However, there have recently been reports of spontaneous layer formation during “step flow” growth of II-VI [16] and Si_xGe_x [17] alloys on highly vicinal surfaces [18,19]. Models to explain this phenomenon are based upon anisotropic elemental attachment probabilities at alternating step edges exhibiting modulated local strain fields [16–19]. Platelet-like short period superlattices have been reported in III-V systems [20]. Layered structures with wavy interfaces, poorly defined periodicity, and increasing surface roughness have also been observed in $\text{Si}_{1-y}\text{C}_y$ layers grown from thermal Si and C beam fluxes [21] as well as from Si evaporated in the presence of C_2H_4 [22]. In all cases, however, the detailed mechanisms leading to self-organized ordering are not well understood.

Here, we report spontaneous natural superlattice patterning controlled by competing surface reactions during alloy film growth by gas-source MBE (GS-MBE). $\text{Si}_{1-y}\text{C}_y(001)$ alloy superlattices, consisting of alternating Si-rich and C-rich layers, are formed during continuous exposure of the growth surface to a constant $\text{Si}_2\text{H}_6/\text{CH}_3\text{SiH}_3$ beam flux. The superlattice structures have highly regular periodicity extending over the entire substrate area, $3 \times 1 \text{ cm}^2$, due to a self-arresting feed-

back loop in the surface-reaction path. Upon initiating film growth, C segregation to the subsurface results in charge transfer from surface dangling bonds to C backbonds which, in turn, significantly decreases the sticking probability of Si_2H_6 . This continues until a critical C coverage is reached allowing nucleation of the second sublayer which is C rich and grows until the excess C is depleted.

All film growth experiments were carried out in a multichamber ultrahigh vacuum system, described in detail in Refs. [23,24], with a base pressure of 5×10^{-11} Torr. The growth chamber, equipped with reflection high-energy electron diffraction (RHEED) and a quadrupole mass spectrometer, is connected through a transfer chamber to an analytical station containing provisions for temperature programmed desorption (TPD), auger electron spectroscopy (AES), and low-energy electron diffraction.

The superlattice structures were grown by GS-MBE from Si_2H_6 and CH_3SiH_3 hydride precursors at 725°C and 750°C . We have shown previously that $\text{Si}_{1-y}\text{C}_y(001)$ GS-MBE at $T \leq 600^\circ\text{C}$, in the surface-reaction limited regime, results in homogenous alloy layers [25,26]. Deposition temperatures T_s used in the present experiments are in the flux-limited regime, well above the H_2 desorption temperature [25]. The Si_2H_6 flux was maintained constant at $J_{\text{Si}_2\text{H}_6} = 2.2 \times 10^{16} \text{ cm}^{-2} \text{ s}^{-1}$ while the average C concentration y_{avg} was varied in separate experiments from 0.0008 to 0.011 by controlling the CH_3SiH_3 flux $J_{\text{CH}_3\text{SiH}_3}$ between 1.9×10^{13} and $7.1 \times 10^{14} \text{ cm}^{-2} \text{ s}^{-1}$. During deposition, the Si_2H_6 and CH_3SiH_3 molecular beams are delivered to the substrate through directed tubular dosers. The dosers are coupled to feedback-controlled constant-pressure reservoirs monitored using capacitance manometers whose signals are in turn used to regulate variable leak valves. Valve sequencing, pressures, gas flows, and film growth temperatures are all computer controlled.

The substrates were 0.5-mm-thick *n*-type Si(001) wafers (resistivity = 10–20 Ω cm) with a miscut of $\approx 0.2^\circ$ along $\langle 110 \rangle$. Initial cleaning consisted of solvent degreasing, multiple wet-chemical oxidation/etch cycles, and a 20 s etch in dilute (10%) HF. The substrates were then exposed to a UV/ozone treatment to remove C-containing species [27] and introduced, through the sample-exchange chamber, into the deposition system where they were degassed at 600 $^\circ\text{C}$ for 4 h, following which they were rapidly heated at $\approx 100^\circ\text{C s}^{-1}$ to 1100 $^\circ\text{C}$ for 1 min to remove the oxide. RHEED patterns from substrates subjected to this procedure were 2×1 with sharp Kikuchi lines. No residual C or O was detected by AES. Si(001) buffer layers were then deposited at 800 $^\circ\text{C}$ prior to commencement of $\text{Si}_{1-y}\text{C}_y(001)$ film growth.

Deposited film thicknesses were measured by microstylus profilometry while C concentrations in as-deposited layers were determined by secondary ion mass spectrometry (SIMS). Quantification, within an experimental uncertainty of $\pm 10\%$, was accomplished by comparison to C ion-implanted bulk Si(001) standards. The $\text{Si}_{1-y}\text{C}_y(001)$ layers contained no detectable impurities. The Cameca IMS-5F spectrometer was operated with a 10 keV Cs^+ primary ion beam and an in-plane raster scan of $250 \times 250 \mu\text{m}^2$. The microstructure and crystalline quality of the layers were investigated using plan-view transmission electron microscopy (TEM), cross-sectional TEM (XTEM), and scanning TEM (STEM) in a JEOL 2010F field emission instrument operated at 200 kV.

Figure 1(a) is a typical XTEM bright-field image, obtained along the $\langle 110 \rangle$ zone axis of a 13-period, 3350- \AA -thick, superlattice structure grown at 750 $^\circ\text{C}$ with an average composition $y_{\text{avg}} = 0.0044$. The image is representative of the entire sample, based upon multiple fields of view and multiple specimens spanning the entire $3 \times 1 \text{ cm}^2$ substrate. The period, $\Lambda = 249 \pm 4 \text{ \AA}$, is highly regular. Figure 2 is a typical SIMS profile from the same sample. The profile consists of 13 bilayers in which every even-numbered sublayer is C rich. The periodicity of the concentration modulation agrees with that of the superlattice periodicity observed in XTEM. SIMS profiles obtained from different regions of the sample were identical. Figure 3 shows that the agreement between XTEM and SIMS determined superlattice periods are equally good for all sample concentrations investigated.

Cross-sectional STEM Z-contrast images obtained using a high-angle annular dark field detector also demonstrate, consistent with the SIMS data, that the dark bands in XTEM images are C rich. Figures 1(b) and 1(c) are higher magnification bright-field XTEM images of the sample corresponding to Fig. 1(a). It is clear that the dark layers are laterally discontinuous consisting of coherent nanoscale C-rich particles of similar size, $\approx 70 \text{ \AA}$ in this case. The particles are coherent, as judged by high-resolution XTEM [see, for example, Fig. 1(c)] showing that the lattice planes are continuous throughout, and do

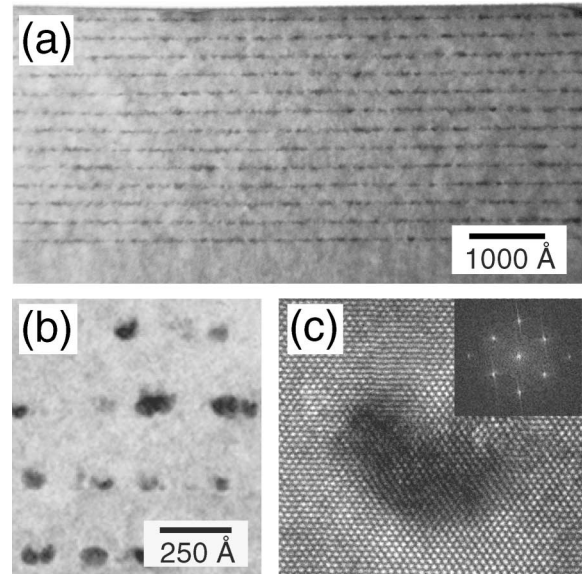


FIG. 1. (a) Bright-field 011 zone axis XTEM micrograph of a $\text{Si}_{1-y}\text{C}_y(001)$ alloy superlattice, with $y_{\text{avg}} = 0.0044$, grown from continuous $\text{CH}_3\text{SiH}_3/\text{Si}_2\text{H}_6$ fluxes at $T_s = 750^\circ\text{C}$. The superlattice period is 249 \AA . (b) Higher magnification XTEM image. (c) High-resolution XTEM image of a C-rich sublayer. The inset is the Fourier transform of the lattice image.

not interrupt film growth. The dark contrast stems from high local strain fields giving rise to differences in Si-Si bond distances between the coherent C-rich particles and the Si-rich matrix.

The inset of Fig. 1(c) is the Fourier transform of the HR-XTEM image. Other than some diffuse scattering around the reflections, the pattern is identical to those obtained from pure Si in agreement with selected-area electron diffraction and nanodiffraction patterns showing that the C-rich particles are commensurate with the Si-rich matrix. A likely candidate for the C-rich phase is Si_4C which was shown by Rucker *et al.* [28], using density functional theory, to be stable in the Si lattice with C occupying ordered third-nearest neighbor sites. The large

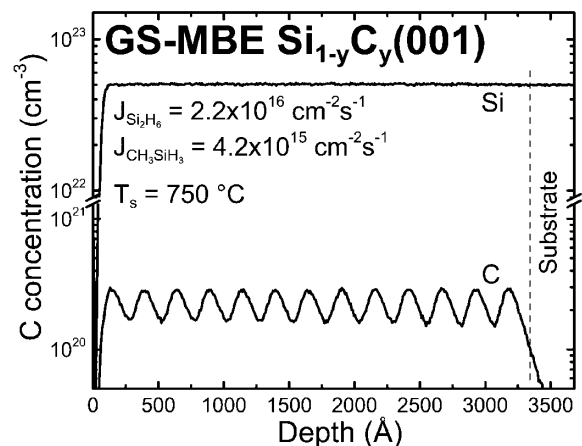


FIG. 2. SIMS depth profile through the superlattice shown in Fig. 1.

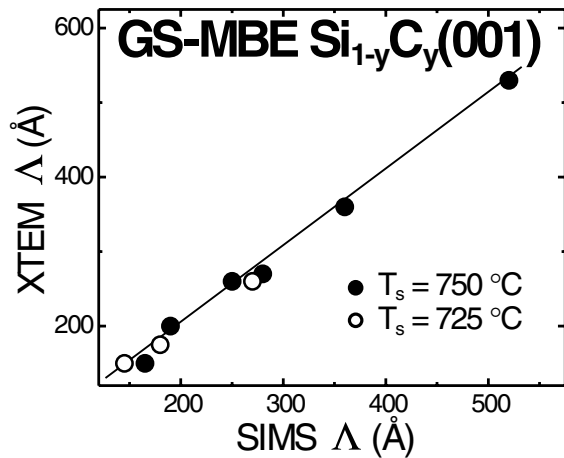


FIG. 3. Superlattice periodicity Λ as measured by XTEM and SIMS for layers grown at 725 °C and 750 °C.

local C concentration required to form this phase would explain the requirement of high growth temperature and strong C segregation to obtain the highly uniform self-organized alloy superlattice shown here.

Figure 4 is a plot of superlattice periods Λ vs y_{avg} and T_s . The continuous decrease in Λ with increasing y_{avg} reflects the fact that the critical C coverage required to nucleate the C-rich layer is achieved more rapidly in samples with higher average C concentrations. Λ ranges from 520 Å with $y_{\text{avg}} = 0.0008$ to 165 Å with $y_{\text{avg}} = 0.011$ at $T_s = 750$ °C. For samples with the same y_{avg} value, Λ decreases with decreasing T_s indicating that C segregation is in the equilibrium regime [29], whereas kinetically limited segregation was observed at $T_s \leq 600$ °C [26].

The spontaneous formation of alloy superlattices with highly regular periodicity and flat interfaces during gas-source $\text{Si}_{1-y}\text{C}_y(001)$ growth at high temperatures can be understood based upon competition among interacting surface reactions. C has a strong tendency to segregate toward the surface and we have shown previously, using

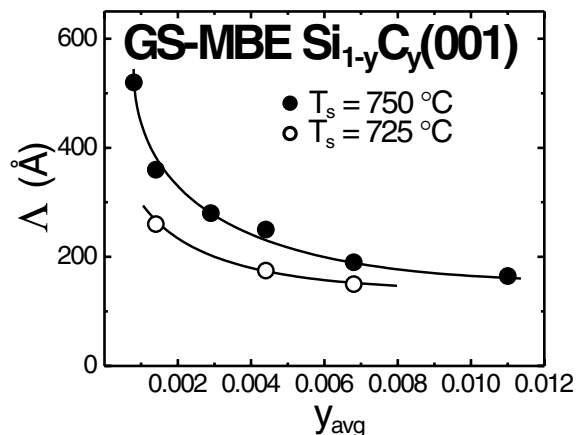


FIG. 4. $\text{Si}_{1-y}\text{C}_y(001)$ alloy superlattice periodicity Λ as a function of y_{avg} for layers grown at 725 °C and 750 °C.

isotopically tagged TPD measurements [25,26], that it prefers to reside in the second, rather than the outermost, layer in order to decrease the strain associated with its small covalent radius (0.77 Å compared to 1.11 Å for Si) combined with the shorter C-Si bond (1.89 Å) [30] with respect to Si-Si (2.35 Å) [30]. The TPD results show that the activation energy for D_2 desorption from Si surface atoms (labeled Si^*) having C backbonds is 0.3 eV lower than that from Si surface atoms with Si backbonds. The energy shift is primarily due to charge transfer, resulting from the higher electronegativity of C, from Si^* dangling bonds to the subsurface $\text{Si}^*\text{-C}$ backbonds together with local strain effects [similar results were reported for ultrahighly B-doped $\text{Si}(001)2 \times 1$ layers in which B is known to preferentially move to the second layer] [31]. This, in turn, leads to a decrease of more than a factor of 70× in the reactive sticking probability of Si_2H_6 at Si^* compared to Si sites and thus a continuous decrease in the film growth R with increasing C segregation [26].

We propose that regular self-organized superlattices form spontaneously during $\text{Si}_{1-y}\text{C}_y(001)$ GS-MBE in the following manner. As film growth is initiated, strong segregation of C to the subsurface yields a continuous increase in the coverage θ_{Si^*} of Si^* surface sites which, correspondingly, gives rise to a continuous decrease in the instantaneous deposition rate R . The decrease in R during the growth of a “Si-rich” layer leads, in turn, to a further enhancement of the C segregation rate and a higher Si^* coverage, resulting in a feedback process which is self-arresting only when θ_{Si^*} reaches a critical value θ_c for the nucleation of a C-rich Si_nC phase. The overall process is illustrated schematically in Fig. 5. When θ_{Si^*} reaches θ_c , a “C-rich” layer is initiated with the growth of fully coherent Si_nC nanoparticles. Continued growth of the C-rich layer decreases θ_{Si^*} and, hence, increases the instantaneous deposition rate R , until the excess subsurface C is consumed. The process then repeats itself to form an alloy superlattice with a highly regular periodicity and flat interfaces over the entire substrate area. The uniformity in the periodicity, we believe, is directly related to the surface-reaction-rate feedback loop which decreases R as θ_{Si^*} is increasing, thus allowing sufficient time for long-range lateral diffusion of subsurface C atoms. This also explains why it is not possible to achieve such uniform periodicity in solid-source MBE $\text{Si}_{1-y}\text{C}_y(001)$ layers where the feedback loop does not exist.

Regarding the chemical nature of the Si_nC nanoparticles, we do not yet have conclusive evidence regarding their composition. Si_4C , which has previously been shown by density functional calculations to be stable in the Si lattice [28], is consistent with our results and would require θ_c to be at least greater than 0.20 ML, with the actual value depending upon the nucleation activation barrier. We can, however, rule out both the hexagonal and cubic polymorphs of SiC based upon HR-XTEM measurements of C-rich nanoparticle interplanar spacings.

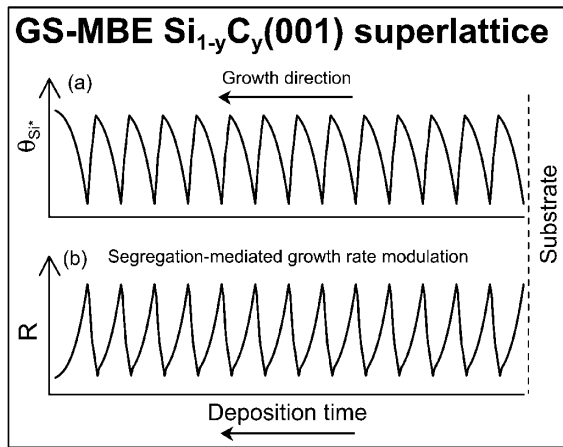


FIG. 5. Schematic diagram showing the coverage of C-backbonded Si surface sites θ_{Si^*} and the instantaneous growth rate R as a function of deposition time during growth of a self-organized $Si_{1-y}C_y(001)$ alloy superlattice.

Finally, we note that the above model for spontaneous superlattice formation also explains our observed $\Lambda(y_{avg}, T_s)$ dependence in a natural manner. Increasing y_{avg} increases the rate of C segregation, thus decreasing the time (i.e., the Si-rich layer thickness) required for θ_{Si^*} to reach θ_c . The y_{avg} dependence of Λ is therefore primarily due to decreases in the Si-rich layer thickness while the C-rich sublayer thickness remains essentially constant as we observe. Increasing T_s in the equilibrium segregation regime decreases the C segregation rate and, hence, increases Λ as shown in Fig. 4.

In conclusion, we present a new pathway for spontaneous superlattice formation based upon competing surface reactions at the growth front during $Si_{1-y}C_y(001)$ GS-MBE. The superlattice structures, consisting of alternating Si-rich and C-rich layers, have highly regular periodicity extending over the entire substrate area due to a self-arresting feedback loop in the surface-reaction pathways. Superlattice periods Λ are tunable through the choice of y_{avg} and T_s .

The authors gratefully acknowledge support of the U.S. Department of Energy (DOE) under Grant No. DEFG02-91ER45439 and the Center for Microanalysis of Materials, partially supported by the DOE.

*Permanent address: Institute of Materials Research and Engineering, 3 Research Link, S(117602), Singapore.

†Permanent address: Korea Research Institute of Standards and Science, Doryong-dong 1, Taejon 305-606, Korea.

[1] N.-E. Lee, D. G. Cahill, and J. E. Greene, Phys. Rev. B **53**, 7876 (1996).

- [2] C. Schelling, G. Springholz, and F. Schaffler, Thin Solid Films **369**, 1 (2000); Phys. Rev. Lett. **83**, 995 (1999).
- [3] J. E. Van Nostrand, S. J. Chey, and D. G. Cahill, Phys. Rev. B **57**, 12 536 (1998).
- [4] A. Vailionis, B. Cho, G. Glass, P. Desjardins, David G. Cahill, and J. E. Greene, Phys. Rev. Lett. **85**, 3672 (2000).
- [5] T. Schwarz-Selinger, Y. L. Foo, David G. Cahill, and J. E. Greene, Phys. Rev. B **65**, 125317 (2002).
- [6] B. Cho, T. Schwarz-Selinger, K. Ohmori, David G. Cahill, and J. E. Greene, Phys. Rev. B **66**, 195407 (2002).
- [7] D. J. Eaglesham and M. Cerullo, Phys. Rev. Lett. **64**, 1943 (1990).
- [8] P. Raiteri, F. Valentinotti, and L. Miglio, Appl. Surf. Sci. **188**, 4 (2002); R. Raiteri *et al.*, Phys. Rev. Lett. **88**, 256103 (2002).
- [9] Y. Fujikawa *et al.*, Phys. Rev. Lett. **88**, 176101 (2002).
- [10] Y. Chen, D. A. A. Ohlberg, and R. S. Williams, J. Appl. Phys. **91**, 3213 (2002).
- [11] J. Nogami *et al.*, Phys. Rev. B **63**, 233305 (2001).
- [12] Y. Chen *et al.*, Appl. Phys. Lett. **76**, 4004 (2000).
- [13] R. P. G. Karunasiri and K. L. Wang, J. Vac. Sci. Technol. B **9**, 2064 (1991).
- [14] K. Nakai, Y. Gotoh, M. Ozeki, and K. Nakajima, Appl. Surf. Sci. **60**, 602 (1997).
- [15] N. Hirashita, J. E. Greene, U. Helmerson, J. Birch, and J. E. Sundgren, J. Appl. Phys. **70**, 4963 (1991).
- [16] S. P. Ahrenkiel *et al.*, Phys. Rev. Lett. **75**, 1586 (1995).
- [17] F. Liu, J. Tersoff, and M. G. Lagally, Phys. Rev. Lett. **80**, 1268 (1998).
- [18] Albert-László Barabási, Appl. Phys. Lett. **70**, 764 (1997).
- [19] P. Venezula *et al.*, Nature (London) **397**, 678 (1999).
- [20] I. T. Ferguson *et al.*, Appl. Phys. Lett. **59**, 3324 (1991).
- [21] For example, H. J. Osten, E. Bugiel, and P. Zaumseil, J. Appl. Phys. **82**, 231 (1997); S. Y. Park, J. D'arcy-Gall, D. Gall, J. A. N. T. Soares, Y.-W. Kim, H. Kim, P. Desjardins, S. G. Bishop, and J. E. Greene, J. Appl. Phys. **91**, 5716 (2002).
- [22] A. Claverie *et al.*, J. Cryst. Growth **157**, 420 (1995); L. Simon *et al.*, Phys. Rev. B **54**, 10 559 (1996).
- [23] D. Lubben, R. Tsu, T. R. Bramblett, and J. E. Greene, J. Vac. Sci. Technol. A **9**, 3003 (1991).
- [24] T. R. Bramblett, Q. Lu, N.-E. Lee, N. Taylor, M.-A. Hasan, and J. E. Greene, J. Appl. Phys. **77**, 1504 (1995).
- [25] Y. L. Foo, K. A. Bratland, B. Cho, J. A. N. T. Soares, P. Desjardins, and J. E. Greene, Surf. Sci. **513**, 475 (2002).
- [26] Y. L. Foo, K. A. Bratland, B. Cho, P. Desjardins, and J. E. Greene, J. Appl. Phys. **93**, 3944 (2003).
- [27] X. J. Zhang, G. Xue, A. Agarwal, R. Tsu, M. A. Hasan, J. E. Greene, and A. Rockett, J. Vac. Sci. Technol. A **11**, 2553 (1993).
- [28] H. Rucker, M. Methfessel, E. Bugiel, and H. J. Osten, Phys. Rev. Lett. **72**, 3578 (1994).
- [29] S. A. Barnett and J. E. Greene, Surf. Sci. **151**, 67 (1985).
- [30] W. Windl, O. F. Sankey, and J. Menéndez, Phys. Rev. B **57**, 2431 (1988).
- [31] H. Kim, G. Glass, T. Spila, N. Taylor, S. Y. Park, J. R. Abelson, and J. E. Greene, J. Appl. Phys. **82**, 2288 (1998).